MICROCT OF CORONARY STENTS: STAINING TECHNIQUES FOR 3-D PATHOLOGICAL ANALYSIS

A Thesis

by

STEPHEN DANIEL DARROUZET

Submitted to the Office of Graduate Studies of
Texas A&M University
in partial fulfillment of the requirements for the degree of

MASTER OF SCIENCE

May 2011

Major Subject: Biomedical Engineering

MicroCT of Coronary Stents: Staining Techniques for 3-D Pathological Analysis

MICROCT OF CORONARY STENTS: STAINING TECHNIQUES FOR 3-D PATHOLOGICAL ANALYSIS

A Thesis

by

STEPHEN DANIEL DARROUZET

Submitted to the Office of Graduate Studies of
Texas A&M University
in partial fulfillment of the requirements for the degree of

MASTER OF SCIENCE

Approved by:

Chair of Committee,	Fred Clubb, Jr.
Committee Members,	Bradley Weeks
	Duncan Maitland
	Matthew Miller
	Mark Lenox
Head of Department,	Gerard Coté

May 2011

Major Subject: Biomedical Engineering

ABSTRACT

MicroCT of Coronary Stents: Staining Techniques for 3-D Pathological Analysis.

(May 2011)

Stephen Daniel Darrouzet, B.S., Texas A&M Unversity

Chair of Advisory Committee: Dr. Fred Clubb, Jr.

In the area of translational research, stent developers consult pathologists to obtain the best and most complete amount of data from implanted test devices in the most efficient manner. Through the use of micron-scale computed tomography along with post-fixation staining techniques in this study, full volumes of previously implanted stents have been analyzed *in-situ* in a non-destructive manner. The increased soft tissue contrast imparted by metal-containing stains allowed for a qualitative analysis of the vessel's response to the implant with greater sensitivity and specificity while reducing beam-hardening artifact from stent struts.

The developed staining techniques included iodine-potassium iodide, phosphomolybdic acid, and phosphotungstic acid, all of which bind to soft tissue and improve image quality through their ability to attenuate high energy X-rays. With these stains, the overall soft tissue contrast increased by up to 85% and contrast between medial and neointimal layers of the vessel increased by up to 22%. Beam hardening artifact was also reduced by up to 38% after staining.

Acquiring data from the entirety of the stent and the surrounding tissue increased the quality of stent analysis in multiple ways. The three dimensional data enabled a comprehensive analysis of stent performance, lending information such as neointimal hyperplasia, percent stenosis, delineation of vessel wall layers, stent apposition, and stent fractures. By providing morphological data about stent deployment and host response, this method circumvents the need to make the more traditional histology slides for a morphometric analysis. These same data may also be applied to target regions of interest to ensure histology slides are cut from the optimal locations for a more in-depth analysis. The agents involved in such techniques are readily available in most pathology laboratories, are safe to work with, and allow for rapid processing of tissue. The ability to forego histology altogether or to highly focus what histology is performed on a vessel has the potential to hasten the development process of any coronary stent.

ACKNOWLEDGEMENTS

I would like to thank my committee chair, Dr. Fred Clubb, and my committee members, Dr. Maitland, Dr. Miller, Dr. Lenox, and Dr. Weeks, for their guidance and support throughout the course of this research. They have provided me with a unique insight to the many facets of my research, which would not have been possible without them.

Thanks also go to my friends and colleagues at the Cardiovascular Pathology Laboratory, especially Jessica Thibodeaux and Aaron Roberts, for providing the assistance I needed on various aspects of my research. I also want to extend my gratitude to Dr. Moore of the Biomedical Engineering Department at Texas A&M for providing me with the samples with which to perform my research. I would additionally like to thank Ralph Nichols at the Texas Heart Institute for assisting in the analysis of my research. I hope my research in turn will be able to return the favor of all those who have helped me.

Finally, thanks to my mother, father, and my entire family for their love and encouragement throughout these many years.

NOMENCLATURE

AUP	Animal Use Protocol
CVD	Cardiovascular Disease
CCD	Charge-Coupled Device
CT	Computed Tomography
FWHM	Full Width at Half Maximum
IVUS	Intravascular UltraSound
I-KI	Iodine-Potassium Iodide
JPEG	Joint Photographic Experts Group
kV	KiloVoltage
MRI	Magnetic Resonance Imaging
μAs	micro-Ampere-seconds
MicroCT	Micron-scale Computed Tomography
NBF	Neutral Buffered Formalin
OCT	Optical Coherence Tomography
PAM	Para-strut Amorphous Material
PMA	PhosphoMolybdic Acid
PTA	PhosphoTungstic Acid
ROI	Region of Interest
SEM	Scanning Electron Microscopy
TEM	Transmission Electron Microscopy

TABLE OF CONTENTS

Page

Page

LIST OF FIGURES

Page

LIST OF TABLES

Page

1. INTRODUCTION

1.1 Cardiovascular Disease and the Need for Stents

Cardiovascular diseases (CVD) accounted for 34.3% of all deaths in 2006 in the United States, making it the leading cause of death (1). Because of the complex nature of the cardiovascular system a multitude of problems can arise during a person's lifetime that can lead to development of CVD. As a result there are a similarly large number of medical devices intended to treat manifestations of CVD in humans. This study focuses on imaging techniques to aid in the development and evaluation of devices intended for a specific area of CVD known as atherosclerosis; however, these techniques can also be applied in a multitude of other areas.

Atherosclerosis is one of the more severe manifestations of CVDs in which lipid material collects within the wall of coronary arteries. This buildup of material can reduce the diameter of the vascular lumen and lead to a reduction in (or complete cessation of) blood flow affecting the downstream myocardial tissue, which is referred to as stenosis. In the late 1970s balloon angioplasty was developed as a treatment option for vessels with such lesions and the procedure included using a catheter with an expandable balloon on the end to expand the artery (2). It was later determined that merely expanding the vessel acutely would not be sufficient to maintain a larger vessel diameter. An expandable metallic scaffold (a stent) was developed to be deployed around the balloon and left inside the vessel (3). The permanent nature of the stent

---

This thesis follows the style of the Journal of the American College of Cardiology.

allowed the vessel to stay patent for a longer period of time but also promoted a chronic inflammatory response from the host. Nevertheless, stents quickly became the therapy of choice for atherosclerosis alongside bypass grafting. Bypass grafting is a more invasive procedure (requiring open heart surgery) compared to catheter-based stent deployment and involves removing a segment of the saphenous vein from a patient's leg and grafting it onto the coronary vasculature in order to bypass a blockage. Since the late 1980s when stents were first being deployed, a plethora of stent types have been developed with different shapes, materials, deployment techniques, mechanical strengths, and drug elution capacities. These current stents along with future devices in development all seek to optimize a variety of parameters dealing with solid mechanics, biochemistry, materials science, fluid mechanics, surgical practices, and manufacturing techniques. These various aspects can be tested individually in the lab and as a whole in animal studies.

1.2 Stent Analyses

In the early design process bench testing can help to determine the mechanical, material, and functional properties of a stent through simulations (i.e. computational fluid dynamics and finite element analysis), test deployments, and manufacturing validations. Computer simulations are useful in determining parameters such as strut shape, width, and spacing (4). While all of these factors are necessary and helpful in designing an optimized stent, bench tests such as these cannot fully predict how the device will perform when deployed in a real vessel. Stents are first deployed in a non-injury animal model to introduce controlled deployment conditions. Through

deployment in living animals one can verify the results of bench testing with more representative data; in addition to being able to collect data regarding how the stent will affect the physiology of the animal. While some performance data can be recorded about the stent *in-vivo* the outcome of the stent deployment relies on a pathological analysis performed after necropsy of the animal.

Stent pathology evaluations are routinely made using traditional histology procedures. The vessels of interest are dissected from the test subject and are processed for routine paraffin histology, plastic embedded histology, scanning electron microscopy (SEM), or transmission electron microscopy (TEM). Each of these traditional evaluative procedures involves examination of selected discrete samples of the stent; whether it is perpendicular to the long axis (histology slides) or parallel to the long axis (SEM). The processes involved in performing plastic histology, for example, on a stented vessel are not only time consuming, costly, and destructive, but commonly leave large areas of the vessel out of the analysis. In order to gather data from the entirety of a vessel, 3-D tomographical imaging techniques can be employed. However, no current imaging technique possesses the sensitivity and specificity that light microscopy-based histology can achieve. The advantage of using a tomographical imaging technique to analyze stents is that the amount of data is vastly increased and is more dynamic, allowing slices to be taken along the entirety of the stent and from different angles. Furthermore, many imaging techniques are non-destructive, allowing data to be collected without precluding the sample from further analysis. Clinical imaging scanners are not typically used in a *post-mortem* stent evaluation due to the limited resolution of the scanners used.

MicroCT uses images of much higher resolutions to provide a more accurate picture of the stent's position and the vessel's healing response. Typically microCT is limited to detecting failed deployments and fractures in the stent struts and (along with injected contrast media) providing data about the lumen of the vessel (5). MicroCT has also been applied to the evaluation of *ex-vivo* test deployments to help explore the effects of over-expansion (6). However, microCT alone lacks the specificity necessary to analyze the vascular tissue around an implanted stent. MicroCT scanners are capable of detecting the densities of vessel tissue, but cannot distinguish between different tissue types in a vessel due to similar densities. Both metrics are necessary to be able to understand how the body is reacting to the implant. Therefore, microCT alone provides little new information other than allowing one to visualize stent fractures, which is merely one manifestation of stent failure. In order to create a more useful microCT stent evaluation technique one must understand and be able to characterize the way a vessel responds to an implant.

While stents play an important role in improving blood flow to a patient's heart they are not without risk both during and after implantation. Two failure modes that are linked to the host response are in-stent restenosis and stent thrombosis. In-stent restenosis is a re-narrowing of the vessel due to trauma from the stent implantation (7). Stent thrombosis is the formation of a thrombus or a blood clot in the coronary vasculature in response to an implanted stent (8). These two outcomes can occur due to procedural problems, manufacturing problems, patient physiology, or intrinsic problems with the stent design. Stent developers in the early design phase can seek to minimize

variability in procedures and patient physiology through using skilled and experienced veterinary cardiovascular surgeons to implant stents in a non-injury animal model. Through controlling the quality of the vessel for implantation as well as the skill of the surgeon developers seek to minimize those variables and focus on aspects of the stent design that may affect its performance, namely the injury induced to the vessel wall. By varying the number of struts in a stent, the shape of the struts, the strut thickness, and the material comprising the stent, the stent may cause different levels of injury to the vessel wall (9). The trauma induced spans a continuum from the vessels being stretched around the stent into a new geometry to a more serious injury scenario where the strut dissects through the vessel wall. After the implantation procedure, damage to the vessel (or a pre-existing lesion, if present) includes denudation of the endothelial lining and possible disruption of smooth muscle cells in the media. The injury can then activate cytokines and other chemotaxic factors that serve to activate smooth muscle cell migration and proliferation (10). This proliferation is a necessary step in order for the vessel to accommodate the stent and eventually heal; however, if the damage is too great the resulting response can be harmful. When smooth muscle cells proliferate excessively it is known as neointimal hyperplasia in general or in-stent restenosis when a stent has been implanted. The neointima that forms in response to a stent often lacks uniform smooth muscle cell orientation and the wall is often expanded by extra-cellular fluid and fibrous connective tissue (10). Depending on the extent of the restenosis the host may be able to remove much of the extra-cellular fluid and reduce the level of restenosis.

Without such a healing process, the restenosis can require intervention as the proliferation can re-occlude the vessel.

An additional phenomenon that is associated with quickly developing neointimal growth is the buildup of para-strut amorphous material (PAM). After a stent is deployed and the endothelial layer of the vessel is damaged, platelets and fibrin can accumulate on and around the struts, causing red blood cells to become enmeshed in them. The endothelial layer then proliferates over the stent struts and the mixture of blood components coalescing in the adjacent area, trapping it within the neointima (11). In areas of normal neointimal growth this PAM can be cleared out through macrophage phagocytosis and digestion of the red blood cells. In thicker areas of neointimal growth macrophages can take a much longer time to reach the PAM and digest the red blood cells, leaving pools of red blood cells near the struts. The other main adverse outcome of stent implantation is the generation of a thrombus due to the stent's presence. Stent thrombi typically begin with the aggregation of platelets and can occur due to a variety of reasons such as changing hemodyamics in the area around the stent struts or the stent material being wholly or partially non-biocompatible. While all of the mechanisms that can lead to a thrombus forming are not well understood there are several patient factors such as diabetes mellitus or resistance to aspirin, and also lesion characteristics such as a particularly long or complex lesion (i.e. bifurcated) that predispose to stent thrombosis (8). Additionally, case-specific implantation complications that can occur include: inappropriate stent sizing and/or expansion, incomplete stent apposition in the vessel, or penetration of a necrotic core. While patient factors such as these are relatively

unchangeable, developers seek to minimize the hemodynamic changes around the stent as well as to prevent poor deployments or stent fractures. Often when biocompatibility appears to be causing problems stent developers will make use of drug-eluting stents coatings while using other materials already being employed in other stents. However, in cases where a new material is being used, even if very similar to other materials, the host could react negatively to the implant. In these cases the device must go through multiple animal trials in order to minimize the host reaction. In order to show a stent can produce a healthy level of neointima while producing no thrombi the stent must be implanted for a given time and then evaluated by a pathologist. Therefore, pathological evaluations of stents tend to focus on identifying weak points in a stent trial to elucidate problems with the stent design.

1.3 Alternative Imaging Techniques

The traditional means of assessing the efficacy of a stent's design and implantation focus on determining the success of the deployment and the level of neo-intimal hyperplasia. Assessing a proper deployment involves knowing where the stent is located and being able to visualize the struts to see if they are structurally sound in relation to the vessel. Measuring the level of neo-intimal hyperplasia involves determining where the medial layer of the vessel ends (i.e. the internal elastic lamina) and how thick the neointimal layer is. Deployment evaluations are presently accomplished *in-vivo* through techniques such as intravascular ultrasound (IVUS)(12), angiography (13), magnetic resonance imaging (MRI) (14), computed tomography (CT) (14), and optical coherence tomography (OCT) (15). *Ex-vivo* analyses then involve

traditional histology procedures such as embedding the vessel in plastic and generating microscope slides for analysis. This slide making technique involves serial sectioning wherein a predetermined number of slides are made from each stent, limiting the analysis to several two-dimensional images. While a large number of slides can be made so as to include representative regions of the whole length of the stent, it is both costly and time consuming, leading most developers to make roughly three to five slides. The slides are then assumed to be representative of the areas of the stent between. This small sample provides an incomplete understanding of the stent's performance. SEM can be used to assess the level of damage to the endothelial layer of the vessel at a given time point by allowing the topography of the inner surface of the vessel to be imaged. However, SEM can be expensive, time consuming, and can prevent the tissue from being analyzed in another fashion (i.e. normal cross-sectional histology slides). SEM provides little data about the level of neointima and other components of the vessel wall. The *in-vivo* methods mentioned above can be used in a *post-mortem* stent analysis as well, but not without limitations of their own. Intravascular ultrasound has been found to lack specificity in distinguishing between tissue types in the vessel wall, in addition to having artifacts induced by dense the metal struts (16). This modality is therefore limited to gross morphological and stent apposition evaluations. While OCT produces finer resolution images than IVUS, it also suffers from strut artifacts and is limited to imaging tissue depths of 1mm (15). Using wavelengths of light near the visible range, OCT is able to determine proper strut coverage and re-endothelialization *in-vivo*, however, the penetration depth limitation of OCT can prevent a complete stent analysis

(15). If the neointimal growth in the vessel is too thick for light from the catheter to reach the medial layer of the vessel proper neointimal measurements cannot be made. Angiography can provide some information about the extent of the neo-intimal hyperplasia by using injected contrast media and in some instances identify fractures in the stent. But it is unable to determine where the medial layer of the vessel is and often lacks resolutions necessary for proper evaluation. Clinical CT and MRI are not typically used for metallic stent evaluations due to the high level of artifacts associated with each imaging modality and the relatively poor resolution compared to the scale of the stented vessel.

1.4 MicroCT Basics and Advantages

To understand how staining soft tissue with radiopaque agents increases both the sensitivity and specificity of a microCT, one must understand how CT and radiographic images are made. CT and plane-film radiographic data are collected by detecting differing levels of attenuated X-ray photons generated by a controlled X-ray source. After being generated from an electron beam aimed at a target (i.e tungsten), X-rays spanning a range of energy levels pass through the sample and strike a flat panel detector (i.e. amorphous silicon) which collects the X-ray radiation and outputs varying levels of visible light based on the remaining energy and amount of X-ray photons after being attenuated by the material. A charge-coupled device (CCD) then detects the photons and converts the data into digital form, creating a digital image of the sample based on the X-ray attenuation values. The attenuation of X-ray photons is a function of the electron density of the various elements contained within the material the photons are passing

through (17). The data collection for radiography and CT is therefore related to the electron density of the elements comprising the object in addition to the object's physical density. Thus, materials with relatively low electron density and physical density, such as most soft tissues, do not attenuate X-rays to a great extent making it difficult for scanners to detect and differentiate between various tissues.

High density materials pose an additional problem during the CT scanning process. Artifacts induced during a CT scan with a metal object occur due to a phenomenon called beam hardening. Beam hardening is a process by which the average energy of a beam of X-ray photons increases as it passes through tissue (16). This increase is possible because many X-ray sources produce a poly-energetic spectrum of X-rays. When the spectrum of X-ray photons pass through an object, lower energy X-rays can become absorbed by the material, only allowing higher energy photons to pass through, increasing the average energy of the remaining X-rays. In cases where X-rays must penetrate a highly dense material such as stainless steel or calcium, many low energy X-ray photons will be absorbed. Depending on the thickness and the type of material, enough photons can be absorbed so that only a small fraction of higher energy X-ray photons pass through to the detector. It is therefore advantageous to increase the starting maximum energy level of the X-ray source to produce a larger number of high energy photons that are capable of penetrating through the dense material. However, as the X-ray energy level increases, soft tissue attenuation decreases. The high energy photons that are able to pass through the material then register a low attenuation from the soft tissue on the opposite side of the material (18). Therefore, increasing the X-ray

energy reduces artifact from metal objects but also diminishes the signal obtained from surrounding soft tissue. Radiopaque staining agents can be used to allow soft tissue to better attenuate the high energy X-rays that are necessary to penetrate a high-density material contained within the soft tissue. Since the late 1980s, there has been much work to reduce or eliminate beam hardening artifacts during or after the reconstruction process (19)(20). With these techniques relying largely on post-processing techniques, there is the possibility of losing some data or having it be interpolated incorrectly (21).

While increasing the X-ray kiloVoltage (kV) during a CT scan helps minimize such artifacts by allowing more photons to penetrate the denser material, it also reduces soft tissue contrast. Therefore, by using radiopaque stains that contain high electron density metals to artificially increase the electron density of the soft tissue, microCTs can be performed on soft tissue with metallic implants at high energy levels. Because the radiopaque staining agents bind to different tissue types with greater or lesser affinities, contrast between different tissue types is possible (Figure 1).

Similar staining agents to the ones evaluated in this study have been used for the purpose of enhancing soft tissue contrast in studies of mouse and chicken models. A variety of different contrast agents, including iodine-potassium iodide (I-KI), phosphotungstic acid (PTA), and osmium tetroxide (OsO_4) have been used to highlight various types of embryonic tissue (22). The staining agents used mainly function by binding to lipids (cell membranes), intracellular proteins, or extracellular proteins and therefore impart a general level of radiopacity relative to the various tissue densities in the tissue (23). Other studies have made use of these agents to create high-contrast

images of small vertebrates and insects (24), rat nephrons (25), rat muscle tissue (26), and pig lungs (27). Post-fixation techniques using similar agents have been created in this study to increase soft tissue contrast and reduce artifacts in coronary vessels containing metallic stents.

Applying post-fixation stains to soft tissue creates a greater sensitivity of the scanner by causing the soft tissue to attenuate more X-ray photons. The stains are all commonly used in histology and gross evaluations and have affinities for slightly different molecules, cell types, and tissues. The relatively heavy metals contained in the stains (iodine, tungsten, molybdenum) are then able to attenuate higher energy X-rays. Because of the binding targets of the stains, the various tissue types contained in a vessel are imparted with different amounts of radiopacity. I-KI or "Lugol's Iodine" is typically used to identify larger polysaccharides at the gross level such as starch-like materials and lipids (28). PTA is a common chemical used in conjunction with hematoxylin in a PTAH fibrin stain along with the similar chemical PMA. These two acidic chemicals are used to stain tissues such as collagen fibers, red blood cells, and muscle fibers (29). PMA has a known lower affinity for binding to tissue while the molybdenum atoms contained in each molecule have a lower electron density and therefore are not as effective at attenuating X-rays. The radiopaque stains can also be combined in order to produce more attenuation under microCT. When PTA or PMA is placed in a solution of water and EtOH for staining purposes, some of the molecules dissociate into a phosphate group and a tungsten (or molybdenum) group. This dissociation lowers the amount of intact PTA or PMA molecules that can bind to the tissue. By combining the two

chemicals in a 2:1 (PTA:PMA) ratio, the PMA is allowed to dissociate, saturates the solution with phosphate groups, which then allows more PTA to bind to the tissue. Additionally, using PTA and PMA to stain tissue first, followed by I-KI staining, can potentially create a large increase in overall radiopacity with the maximum amount of tissue being stained.

While the staining agents may have different binding properties, the staining process functions by attaching heavy metals to proteins, lipids, and other molecules in the tissue. The metal that is deposited is then much more radiopaque than the tissue itself and causes a larger amount of photons to be attenuated to a greater extent. This greater attenuation increases the soft tissue contrast during microCT. By scanning the full volume of the stent after staining, various regions of tissue in the vessel along with the structure of the implanted stent itself can be evaluated from the same dataset.

2. MATERIALS AND METHODS

2.1 Materials

Research was carried out at the Texas A&M University Cardiovascular Pathology Laboratory in College Station, Texas in cooperation with the Department of Biomedical Engineering and the Department of Veterinary Pathobiology. The study included porcine iliac vessels with implanted metal stents as part of a separate study (AUP#:2005-102). This project was carried out between October of 2010 and March of 2011. The following is a description of the materials and equipment used in this research project.

All porcine samples were received from necropsy having been fixed *in-situ* using 10% neutral buffered formalin (NBF) in plastic specimen jars. Samples were scanned using an X-Tek HAWK 160XI combined X-ray and microCT scanner (made by Nikon Metrology, Inc.). The raw microCT data was then transferred via external hard drive to a dedicated reconstruction computer. The computer made use of proprietary reconstruction software (CT-Pro) to generate microCT datasets, which were then viewed using VGStudioMAX (made by Volume Graphics, GmbH). Reconstructed volumes contain CT numbers on a 16-bit color scale, with values ranging from 0 to 65,536.

Samples were stained with three chemicals: I-KI (aqueous solution), PTA (aqueous solution), and PMA (solid crystal in solution) in different concentrations and in different base solutions depending on the chemical. In processing for microground histology, samples were dehydrated using ethyl alcohol (EtOH) and then infiltrated with

technovit 7200, a methyl methacrylate light-activated polymer. Sample preparation made use of a shaker table, dessicator, and light-polymerizer. Slides were then cut and ground using a diamond band saw and microgrinder system (made by EXAKT GmbH). The slide staining process made use of formic acid, ethyl alcohol, Scott's tap water, Gibb's hematoxylin, eosin, and phyloxine B to produce a traditional H&E stain on a plastic slide.

Slides were scanned into digital format using a Nikon Super Cool Scan 9000. Unstained material within slides was sent to the Texas Heart Institute at the University of Texas Medical School at Houston for analysis using an XLT ultramicrotome to cut samples, toluidine blue, basic fuchsin, uranyl acetate, and lead citrate to stain the samples, and a JEOL 1230 electron microscope with an AMT 600 digital camera to image the samples. Slide images and microCT data were analyzed using ImageJ (NIH) image analysis software, Image-Pro (Media Cybernetics) software, and Microsoft Excel (Microsoft Corp.).

2.2 Selection of Radiopaque Staining Chemicals

In order to carry out this research, chemicals were first selected and tested based on their safety, cost, and effectiveness before being applied to the stented vessels for this study. OsO_4 was eliminated as a possibility due to the high cost of the chemical in addition to its high toxicity even in small amounts. I-KI, PTA, and PMA were therefore chosen for the project. In addition to testing the chemicals alone, combined stains of PTA & PMA and PTA, PMA, & I-KI were evaluated.

2.3 Individual Staining Trials

Before testing each chemical on stented vessels increasing concentrations of each chemical were used to stain non-stented porcine vessel tissue. In order to quickly determine the relative level of radiopacity added by each chemical radiographs were taken before and after each trial and at different time points during the staining process. Each staining chemical was tested on its own at first, followed by combination stains. For the PTA staining trials the tissue was first dehydrated to 70% EtOH due to the evidence showing the PTA stain has been shown to function best in that solution (29). PTA solutions of 0.5%, 1%, and 5% in 70% EtOH were prepared and the samples were placed in the chemical over night. At 24 and 48 hours of staining radiographs were taken of each sample at the same X-ray power settings. A similar process was used for the analysis of PMA as a staining chemical. 0.5%, 1%, and 5% solutions were prepared and images were collected at 24 and 48 hours. For I-KI, the staining process included no EtOH and the samples were stained in an aqueous solution of 5% I-KI, 10% I-KI, and 10% I-KI with additional added potassium iodide (KI) to buffer the solution. Samples were stained for and imaged at 24 and 48 hours. The radiographic images collected were then analyzed in ImageJ. Contrast percent for this study was calculated as follows:

$$\text{Contrast Percent} = \frac{(AU_O - AU_B)}{(AU_O - AU_B)/2}$$

where AU_O is the arbitrary unit gray value for the object, and AU_B is the arbitrary unit gray value for the background. In addition to the contrast percent (Table 1), images

were inspected visually to qualitatively judge the increased specificity created by the stain in different parts of the tissue.

Table 1. Staining concentration trials			
	0.5% Stain Measured Contrast Percent	1% Stain Measured Contrast Percent	5% Stain Measured Contrast Percent
PTA Test Sample	19	51	57
PMA Test Sample	16	23	27
I-KI Staining concentration trials			
	5% Stain Measured Contrast Percent	10% Stain Measured Contrast Percent	10% with 5g KI Stain Measured Contrast Percent
I-KI Test Sample	29	59	45

After such analysis it was determined that 3% PTA, 3% PMA, and 10% I-KI were optimal staining concentrations. A concentration of 3% was chosen for the PTA and PMA samples due to the fact that the 1% stain had not imparted enough stain to the vessels yet a 5% stain caused the solution to dehydrate the tissue to a large extent and caused shrinkage of the vessel.

Prior to staining stented porcine vessels for this study each vessel had been fixed in 10% NBF. Unstained scans were then completed at 150kV and 134 µAs with an 8mm aluminum plate used to pre-harden the X-ray beam. Approximately 1000 projections were taken per vessel, creating an average resolution 18µm. After scanning and reconstruction of each unstained vessel, the vessels were stained according to the optimal staining procedure determined previously. Vessels were removed from staining chemicals and placed in a plastic sample pouch filled with either 70% EtOH or distilled

water in order to prevent dehydration during the scanning process. All vessels were then placed in 70% EtOH and processed for plastic microground histology.

In comparing staining times between the different staining trials, it was noted that the stains containing PTA and/or PMA required at least 48 hours of staining time to sufficiently penetrate the majority of the tissue. Initially, the I-KI stain was performed on this same timescale, however due to a perceived faster staining time a second I-KI trial was initiated in which the staining process was more closely monitored over time. Thus, another advantage of the I-KI stain was found to be its ability to penetrate the soft tissue of the vessels in roughly 3 hours.

2.4 Combined Staining Trials

In order to explore possible advantages of combining some of the staining chemicals, given that they have slightly different binding affinities, combination stains were tested and analyzed alongside the individual staining trials. A PTA & PMA stain in a ratio of 2:1 was compared with the 3% PTA and 3% PMA data due to PMA's ability to provide buffer for PTA and allow more stain to bind to the tissue. Additionally, all three chemicals were combined in a trial to explore differences in the types of tissue being stained within a single sample. Vessels were prepared by performing a microCT scan prior to staining. The vessels were then stained with the combinations PTA & PMA and PTA, PMA & I-KI using 3% PTA, 1.5% PMA, and 10% I-KI. Vessels were removed from staining chemicals and placed in a plastic sample pouch filled with either 70% EtOH or distilled water in order to prevent dehydration during the scanning process. The vessels were scanned using the same power settings (150 kV, and

134μAs), taking approximately 1000 projections and resulting in an average resolution of 18μm. The vessels were then placed in 70% EtOH and processed for plastic microground histology.

2.5 Volume Analysis

Upon completion of the reconstructions the microCT volumes were analyzed using VGStudioMAX and Image-Pro. The scans were visualized in three different slice views as well as a 3-D rendered volume. The 3-D volume allows for better visualization of the shape of the vessel and stent as a whole, whereas the slice views were used to create comparable images for validation with histology. The volumes of each vessel were analyzed for regions of interest (ROIs) that were representative of the sample. Average CT numbers were calculated from ROIs of the background (air), neointima, media, stent struts, and areas of high stain uptake in the vessel wall. Slices of the stent with identifiable areas of stent deformation, high levels of neo-intimal hyperplasia, or other sites of high stain uptake were taken note of and targeted for histology. The axial slices that contained these areas of interest were exported from the program and saved as Joint Photographic Experts Group (JPEG) image files. In addition to axial slice images showing the stained soft tissue surrounding the stent struts, images of the same slice with the density window adjusted to the full width at half maximum (FWHM) of the stent strut data were collected. A similar analysis was performed on the unstained sample data with average CT numbers being calculated from ROIs generated approximately in the neointima and media. The stained images were then imported into Image-Pro software, which enables measurements to be taken on the images. The measurement

function of the software was calibrated by using the images showing the stent struts at FWHM (Figure 2) which were manufactured to be 150µm. The calibration made use of the FWHM view of the struts in order to approximate the size of the stent struts. Lumen circumference, stent circumference and medial circumference measurements were taken as a means to compare the quantitative capabilities of microCT slice data for stent tissue analysis (Figure 3). An example of the measurements is shown in Table 2.

Table 2. Measurement data from histology and microCT images

	Histology Slide Measurements (mm)	MicroCT Slice Data Measurements (mm)
Lumen Circumference (Red Circle)	9.19	7.95
Stent Circumference (Yellow Circle)	16.08	14.95
Media Circumference (Green Circle)	17.34	15.84

2.6 Plastic Histology

After completion of the staining and scanning process for each of the 5 vessels, the tissue continued the dehydration process in preparation for plastic histology. The samples were placed on a shaker table in graded alcohols until 99% was reached. The vessels were then infiltrated with the liquid form of a light polymerizing methyl methacrylate, Technovit 7200 (Exact) by graded infiltration in EtOH. After standard infiltration times for stented vessels, they were placed in a light polymerizer to harden the polymer. Slides were then cut from the embedded tissue using an EXACT diamond band saw system. The slides chosen were based on the areas of interest as seen in the

microCT data and were cut as close to those regions of interest as possible. The slides were then ground to a useful thickness ranging from 25-75μm. Once polished, some slides maintained their radiopaque chemical stain and did not require histological staining, others were stained using an H&E staining protocol developed for plastic histology.

2.7 Histological Analysis

In order to validate the microCT data and ensure that the various areas of tissue shown in the microCT data are representative of the tissue, the histology slides were analyzed using the same morphometric parameters as the microCT slice data. Using a Nikon Super Cool Scan 9000 digital versions of each slide were made at 2x magnification. For calibration a standardized micrometer slide was scanned and digitized in the same fashion. The images were stored as JPEGs and imported into Image-Pro software for analysis. Using the calibration slide image to ensure the measurements were accurate the lumen circumference, stent circumference, and medial circumference were measured and tabulated (Table 2). Additionally, the areas of high stain uptake identified in microCT slice data were brought to pathologists for identification. Due to the microCT staining agents interfering with the H&E histology staining of some cellular types, some areas were not able to be identified. These samples were then taken to the Texas Heart Institute for TEM analysis. Slides containing high radiopaque stain uptake material that could not be stained with H&E stains were analyzed with a JEOL 1230 electron microscope (JEOL USA, Inc.) and images captured with an AMT 600 digital camera. The samples were prepared by identifying an area of

interest and removing it from the slide, which was then placed in plastic resin from which thick (1µm) and thin (80-90nm) sections were cut on an ultramicrotome. Thick sections were stained with toluidine blue and basic fuchsin. Thin sections were mounted on 100 mesh copper grids and stained with uranyl acetate and lead citrate. The sections were then examined on an electron microscope. The resulting TEM images were then reviewed by a pathologist with experience in vascular TEM analysis for identification of the material.

3. RESULTS

3.1 Layout of Analysis

There were many aspects of this study that must be examined in order to make decisions about the utility of the proposed techniques. The radiopaque stains aim to increase the sensitivity and specificity of the microCT process in an efficient and non-destructive manner. It is therefore necessary to compare the stains to each other through the relative radiopacity they impart to the vessels. Furthermore, the radiopaque stains must be compared to the resulting histology through their ability to stain certain tissue types representatively. Additionally, the stains must be evaluated for their speed of staining and the vessel's ability to still be used in traditional histology if desired. Through exploring the strengths and weaknesses of the staining chemicals one can determine the most useful microCT staining technique.

The staining process must itself be verified and shown to have increased the radiopacity of the vessel while also decreasing the level of metal streaking artifact. An increase in radiopacity is measured by comparing the contrast level in ROIs from the stained data to similar ROIs in the unstained data. The level of artifact present before and after scanning is represented by the change in standard deviation of the CT numbers detected within the metal of the stent and its adjacent volume. After comparing the level of radiopacity added to the vessel tissue the stains can then be compared to each other in order to determine which chemicals increase the soft tissue contrast to a larger extent.

3.2 Contrast Increase Due to Staining

After calculating contrast levels within the stained and unstained data sets, the contrast percent increase was calculated for each stain trial (Table 3).

Table 3. Summary of contrast increase after 48 hours of staining

	PTA	PMA	I-KI	PTA & PMA	PTA, PMA, & I-KI
Neointima Contrast Increase	28%	21%	64%	56%	63%
Media Contrast Increase	57%	31%	85%	73%	85%
Strut CT Number Standard Deviation Decrease	32%	15%	38%	28%	36%

By looking at the values in table 3, one can see that all of the stains helped to increase the contrast of the vessel, however not all stains were able to differentiate sufficiently between tissue types, namely the media and neointima of the vessel. The standard deviation of the CT numbers in the area surrounding the stent strut are representative of whether the stained tissue surrounding the stent struts is able to attenuate the scattered X-ray photons thereby masking the scattered photons. The PTA stain provided a 57% increase in the contrast of the medial layer of the vessel and was able to clearly delineate the lumen of the vessel (Figure 4). The standard deviation of the CT numbers surrounding the struts in the PTA stain decreased by 32% after staining, indicating that there was a significant drop in the level of metal artifact. The PMA stain showed a slight increase in contrast overall, but did not allow for a clear distinction

between media and neo-intima (Figure 5). In figure 5 the left image shows that the PMA stain was also unable to penetrate the full thickness of the tissue, despite having been allowed to stain the tissue for 48 hours. Furthermore the PMA stain decreased the standard deviation of the CT numbers by the lowest amount, causing metal artifact streaks to remain. The I-KI stain was able to increase the soft tissue contrast of the vessel by 85% for the media and allowed for a large decrease in the level of metal artifact (Figure 6). The 48 hour I-KI stain, while proving to be a powerful tool for aiding in microCT data collection also prevented the tissue from being sectioned with plastic histology. The 3 hour I-KI stained vessel was placed back in formalin upon completion of the scan, which removed the I-KI from the tissue and allowed for normal plastic histology (Figure 7). The combined PTA & PMA stain was able to increase the contrast of the tissue overall, provided better contrast than the PTA or PMA stains alone, and reduced the metal artifact roughly the same amount as the PTA stain alone. However, this combined stain did not produce as much of a contrast change between the media and neointima (Figure 8). Finally, the combined PTA/PMA/I-KI produced a similar contrast increase to the I-KI stain alone, and it was able to reduce the metal artifact roughly the same amount. This would suggest that the I-KI solution possibly replaced the PTA and PMA staining molecules in the tissue. However, as with the other I-KI sample, the stain was not removed prior to processing and thus the tissue was not penetrated properly for plastic histology (Figure 9).

3.3 Verification with Histology

The axial slices and measurements of each vessel's scan data were compared with the histology slides and measurements. In order to accurately measure histology slides that had been digitized by a Nikon Super Cool Scan 9000 digital slide scanner a calibration slide was used to set the exact number of millimeters per pixel (mm/pixel) for all slides scanned with the scanner. Because of technical complications with spatial calibrations of the microCT scanner, the CT slice data was similarly calibrated from the FWHM axial view images to be 150μm. The CT slices analyzed were captured at the slice most closely approximating where the histology slides were cut in order to ensure the most appropriate juxtaposition of measurements. CT and histology measurements were compared plotted against one another in Microsoft Excel where a linear regression showed a close correlation between the slice data measurements (Figure 10).

The variations between the measurements can be partially attributed to the staining process itself and whether or not the samples were dehydrated before scanning. Samples stained with I-KI were stained in an aqueous solution whereas the PTA and PMA samples were stained in a 70% EtOH solution, partially dehydrating the tissue and causing shrinkage. The highly acidic nature of PTA and PMA solutions may also have caused a higher level of tissue shrinkage during the staining process that was then rectified when the tissues were processed for histology. There is also some geometric distortion affecting the measurements wherein both the microCT scanning process and the plastic histology process are not able to produce slices perfectly perpendicular to the long axis of the stent. The slight angles that both the histology slides and microCT slices were taken at may have then skewed the measurements slightly. Even with such

variations when compared to histology, the ability to take such measurements from every slice in a volume of CT data allows this method to be a useful qualitative tool for identifying areas of concern and interest within a stented vessel.

3.4 Detection of PAM

It was also noted in analyzing the microCT data that in places of high neointimal proliferation there were high levels of stain uptake in both the acid based stains and the iodine-based stains (Figure 11). These areas were not able to be stained with normal histology chemicals (Figure 11). This lack of normal staining is perhaps due to the chemical changes that took place during the microCT staining process. In order to identify the material samples were sent to THI for TEM analysis, which showed the areas to be pools of red blood cells having formed next to the stent struts, indicating the areas contained PAM (Figure 12). These areas had some of the highest affinities for both PTA and I-KI and therefore had increased contrast levels compared to the other types of tissue (25% above that of the media). Because not all the samples in this study contained such material, the relative abilities of each stain to detect PAM in the vessel wall could not be included in as a method of comparing each staining technique. However, the ability to detect such material could be evaluated at a future time.

4. DISCUSSION AND CONCLUSION

The process of fine-tuning a device to optimize the performance after implantation can involve multiple animal studies, all of which must be analyzed by a pathologist. By maximizing the amount of data from animal studies one can help to minimize the cost and time between design changes and therefore minimize the time to market for the next generation of any device. The power of using the described microCT staining techniques is in the ability to rapidly perform a full analysis of the tissue in a non-destructive way. While the resolution of microCT has not achieved that of light microscopy and therefore cannot be used as a diagnostic tool for individual cell types, qualitative characterization of the stent remains a useful form of analysis. The ability to gather data from the entirety of the stent and analyze it for medial dissections, stent apposition problems, stent fractures, etc. allows one to quickly distinguish between neointimal hyperplasia due to a medial dissection or due to an intrinsic design flaw. In cases where a problem occurs that is external to the stent design (i.e. poor stent apposition), identification of that problem through microCT could lower the need to perform traditional histology on the vessel, thereby saving both time and money by avoiding a histological analysis that would yield little or no useful data.

After analyzing the effectiveness of the various staining methodologies, it is clear that I-KI is the most useful and rapid stain. The tissue, once fixed in formalin, can be placed directly into the I-KI solution with no dehydration required. The stain time for I-KI to penetrate roughly 2mm of vessel tissue was found to be 3 hours. Taking into

account staining, scanning, and reconstruction, the total time to perform a full microCT analysis of the entirety of the stent is approximately 5 hours. The vessel can then be placed back in formalin over night to remove the I-KI and can then be dehydrated and be prepared for traditional plastic histology. By comparison, the dehydration process alone for a stented vessel in plastic histology can take 8 hours with the rest of the process requiring days before slides can be analyzed. One of the disadvantages of using I-KI is its relative lack of specificity when other tissues are involved. Because I-KI binds readily to lipids, any sample with excessive fatty tissue surrounding the area of interest can become saturated and obstruct the distinction between the layers of the vessel wall. This phenomenon could become a problem in human samples that contain larger amounts of lipid material. Therefore, in cases where there is a large amount of extraneous tissue surrounding the sample, the PTA stain would be preferable due to the high amount of contrast added to the tissue and its lack of ability to stain lipids.

A further powerful use of such staining techniques stems from the identification of PAM within the vessel wall. Being able to characterize and possibly quantify the level of red blood cells captured in the para-strut areas after implantation could help to understand the way PAM develops and the way it heals over time. Additionally, with the knowledge of how effectively the staining chemicals are taken up by red blood cells, one would be able to analyze stented vessels that are difficult if not impossible to be analyzed through other CT methods. When *post-mortem* blood remains in the vessel lumen after dissection traditional CT methods of imaging are not possible due to the inability to inject contrast media into the lumen and the inability to distinguish blood

from the vessel wall. Furthermore, the possibility of distinguishing between *post-mortem* blood and thrombi in the vessel would be possible through this technique, removing yet another reason for vessels to undergo traditional histology. Other possible diagnostic capabilities of such techniques include identification of areas of necrosis or fibrosis, but these remain to be tested in the future.

REFERENCES

1. D Lloyd-Jones, RJ Adams, TM Brown, M Carnethon, S Dai, and G De Simone. Heart disease and stroke statistics 2010 update: a report from the american heart association. Journal of the American Heart Association, 2010;121(12):204. [PubMed 20019324]

2. Gruntzig AR, Senning A, Siegenthaler WE. Nonoperative dilatation of coronary-artery stenosis: percutaneous transluminal coronary angioplasty. New England Journal of Medicine 1979;301(2):61-8. [PubMed: 449946]

3. Sigwart U, Puel J, Mirkovitch V, Joffre F, Kappenberger L. Intravascular stents to prevent occlusion and restenosis after transluminal angioplasty. New England Journal of Medicine. 1987;316(12):701-6. [PubMed 2950322]

4. Timmins LH, Moreno MR, Meyer CA, Criscione JC, Rachev A, Moore JE. Stented artery biomechanics and device design optimization. Medical and Biological Engineering and Computing. 2007;45(5):505-13 [PubMed 17375345]

5. Foerst J, Ball T, Kaplan A. Postmortem in situ micro-CT evaluation of coronary stent fracture. Catheterization and Cardiovascular Interventions. 2010;76(4):527-31. [PubMed 20882657]

6. Basalus MWZ, van Houwelingen KG, Ankone MJK, Feijen J, von Birgelen C. Micro-computed tomographic assessment following extremely oversized partial postdilatation of drug-eluting stents. EuroIntervention. 2010;6(1):141-8 [PubMed 20542810]

7. Edelman ER, Rogers C. Pathobiologic responses to stenting. American Journal of Cardiology 1998;81(7A):4E-6E. [PubMed 9551587]

8. Holmes DR, Kereiakes DJ, Garg S, Serruys PW, Dehmer GJ, Ellis SG, Williams DO, Kimura T, Moliterno DJ. Stent thrombosis. Journal of the American College of Cardiology. 2010;56(17):1357-65. [PubMed 20946992]

9. Garg S, Serruys PW. Coronary stents: looking forward. Journal of the American College of Cardiology. 2010;56(10):S43-78. [PubMed 20797503]

10. Garg S, Serruys PW. Coronary stents: current status. Journal of the American College of Cardiology. 2010;56(10):S1-42. [PubMed 20797502]

11. Farb A, Heller PF, Shroff S, Cheng L, Kolodgie FD, Carter AJ, Scott DS, Froehlich J, Virmani R. Pathological analysis of local delivery of paclitaxel via a polymer-coated stent. Circulation. 2001;104(4):473-9. [PubMed 11468212]

12. Kang SJ, Mintz GS, Park DW, Lee SW, Kim YH, Lee CW, Han HM, Kim JJ, Park SW, Park SJ. Tissue characterization of in-stent neointima using intravascular ultrasound radiofrequency data analysis. American Journal of Cardiology. 2010;106(11):1561-5 [PubMed 21094355]

13. Ganguly A, Simons J, Schneider A, Keck B, Bennett NR, Herfkens RJ, Coogan SM, Fahrig R. In-vivo imaging of femoral artery nitinol stents for deformation analysis. Journal of Vascular Interventional Radiology. 2011;22(2):244-9. [PubMed 21276917]

14. Nordmeyer J, Gaudin R, Tann OR, Lurz PC, Bonhoeffer P, Taylor AM, Muthurangu V. MRI may be sufficient for noninvasive assessment of great vessel stents: an in vitro comparison of MRI, CT, and conventional angiography. American Journal of Roentgenology. 2010;195(4):865-71. [PubMed 20858811]

15. Guahliumi G, Sirbu V. Optical coherence tomography: high resolution intravascular imaging to evaluate vascular healing after coronary stenting. Catheterization and Cardiovascular Interventions. 2008;72:237-47. [PubMed 18655155]

16. Thim T, Hagensen MK, Wallace-Bradley D, Granada JF, Kaluza GL, Drouet L, Paaske WP, Bøtker HE, Falk E. Unreliable assessment of necrotic core by virtual histology intravascular ultrasound in porcine coronary artery disease. Circulation: Cardiovascular Imaging. 2010;3(4):384-91. [PubMed 20460496]

17. Bushberg JT, Seibert JA, Leidholdt EM Jr., Boone JM. The essential physics of medical imaging. Philadelphia, PA: Lippincott Williams & Wilkins. 2002. 369-75.

18. Duerinckx AJ, Macovski A. Nonlinear polychromatic and noise artifacts in X-ray computed tomography tmages. Journal of Computer Assisted Tomography. 1979;3(4):519-26. [PubMed 457966]

19. Kalender WA, Hebel R, Ebersberger J. Reduction of CT artifacts caused by metallic implants. Radiology. 1987;164:576-7. [PubMed 3602406]

20. Prell D, Kyriakou Y, Kachelrie M, Kalender WA. Reducing metal artifacts in computed tomography caused by hip endoprostheses using a physics-based approach. Investigative Radiology 2010;45(11):747-54. [PubMed 20661145]

21. De Man B, Nuyts J, Dupont P, Marchal G, Suetens P. Metal streak artifacts in X-ray computed tomography: a simulation study. Nuclear Science. 1999;46(3):691-6.

22. BD Metscher, MicroCT for developmental biology: A versatile tool for high contrast 3D imaging at histological resolutions. Developmental Dynamics. 2009;238:632-40. [PubMed 19235724]

23. Nagase T, Sasazaki Y, Kikuchi T, Machida M. Rapid 3-dimensional imaging of embryonic craniofacial morphology using microscopic computed tomography. Journal of Computer Assisted Tomography. 2008;32(5):816-21. [PubMed 18830118]

24. Metscher BD. MicroCT for comparative morphology: simple staining methods allow high-contrast 3D imaging of diverse non-mineralized animal tissues. BMC Physiology 2009;9(11):1-14. [PubMed 19545439]

25. Bentley MD, Jorgensen SM, Lerman LO, Ritman EL, Romero JC. Visualization of three-dimensional nephron structure with microcomputed tomography. The Anatomical Record. 2007;290(3):277-83. [PubMed 17525936]

26. Jeffery NS, Stephenson RS, Gallagher JA, Jarvis JC, Cox PG. Micro-computed tomography with iodine staining resolves the arrangement of muscle fibers. Journal of Biomechanics. 2010;44(1):189-92. [PubMed 20846653]

27. Litzlbauer HD, Neuhaeuser C, Moell A, Greschus S, Breithecker A, Franke FE, Kummer W, Rau WS. Three-dimensional imaging and morphometric analysis of alveolar tissue from microfocal X-ray computed tomography. Innovative Methodology. 2006;291(3):L535-45. [PubMed 16679382]

28. Epstein JB, Scully C, Spinelli J. Toluidine blue and Lugol's iodine application in the assessment of oral malignant disease and lesions at risk of malignancy. Journal of Oral Pathology & Medicine. 1991;21(4):160-3. [PubMed 1376363]

29. Kiernan JA. Histological and histochemical methods theory and practice 4th edition. Bloxham, UK: Scion Publishing. 2008:192-208.

APPENDIX

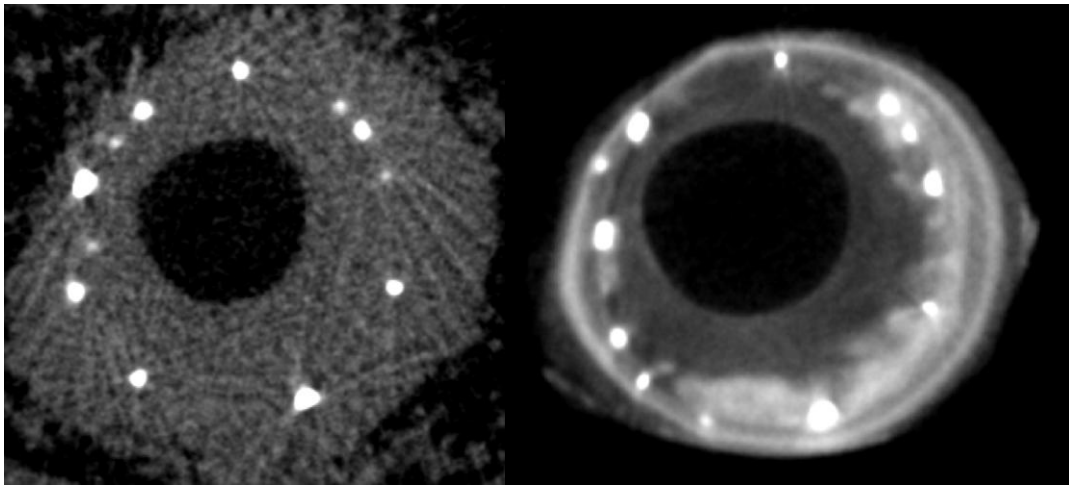

Figure 1. Effects of Staining on Stented Vessels
MicroCT slice images of before (left) and after (right) radiopaque staining techniques to show the increased quality of data through staining.

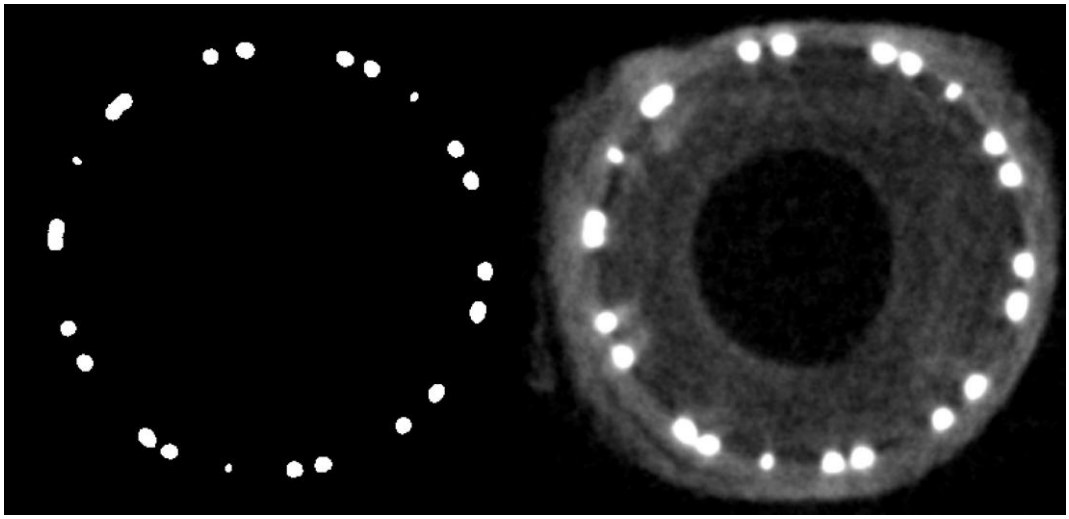

Figure 2. Slice Images Used for Calibration
MicroCT slice images showing just the metal struts at FWHM (left) for calibration of Image-Pro and the same slice with the tissue being displayed (right) for measurements.

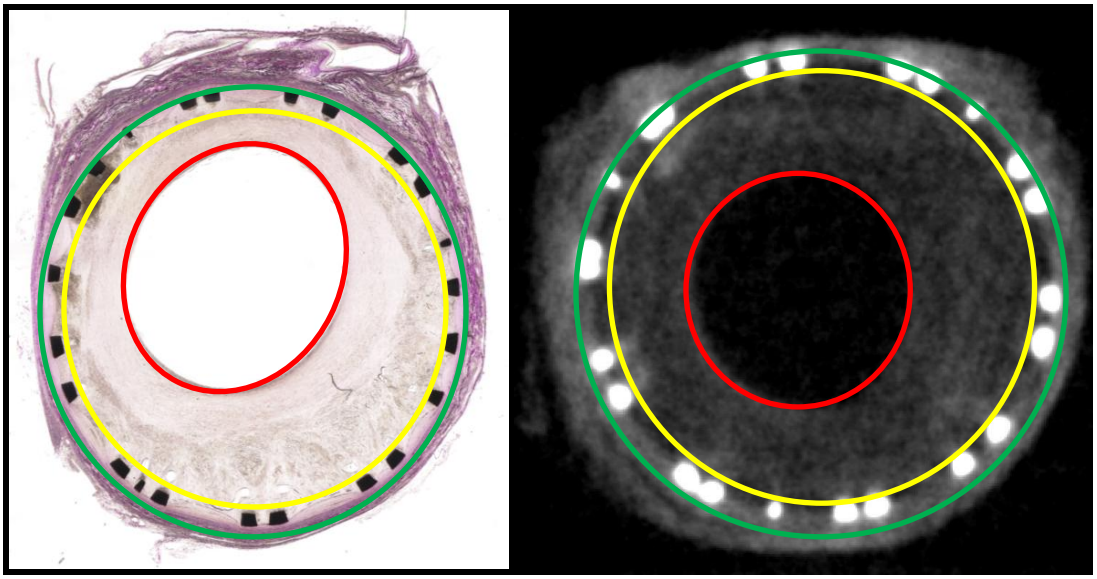

Figure 3. Measurements of Histology and MicroCT Slice Data
Images showing technique for comparing measurements between histology and microCT slices. The circles shown on the pictures are representative of where the measurements were taken and correspond to the measurements in table 6.

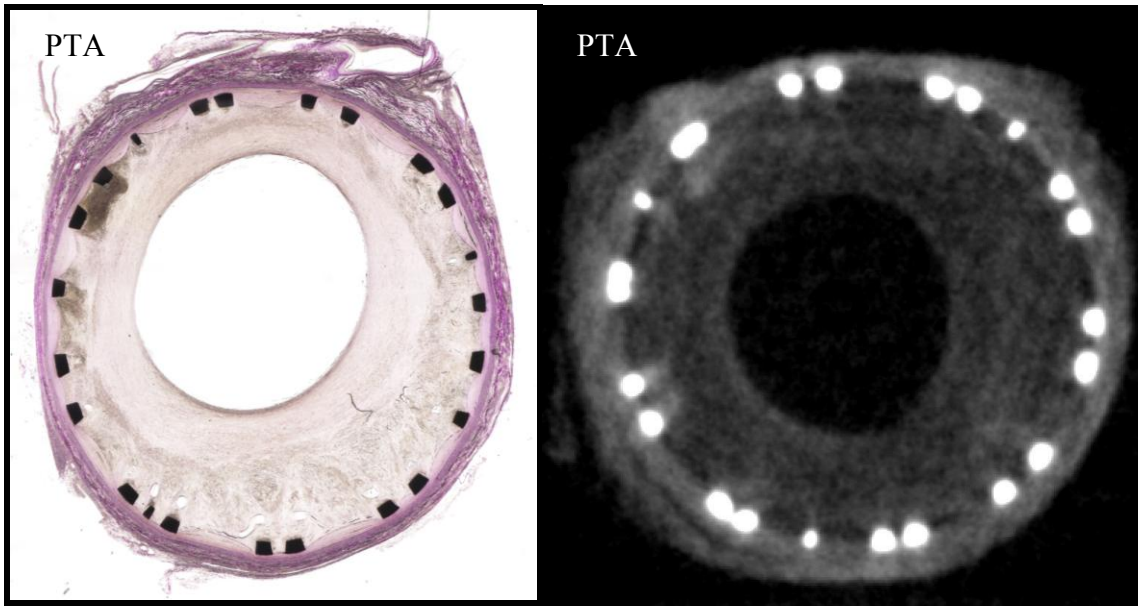

Figure 4. PTA Staining for 48 Hrs
Comparison of histology (left) and microCT slice view (right) of a vessel having been stained with PTA.

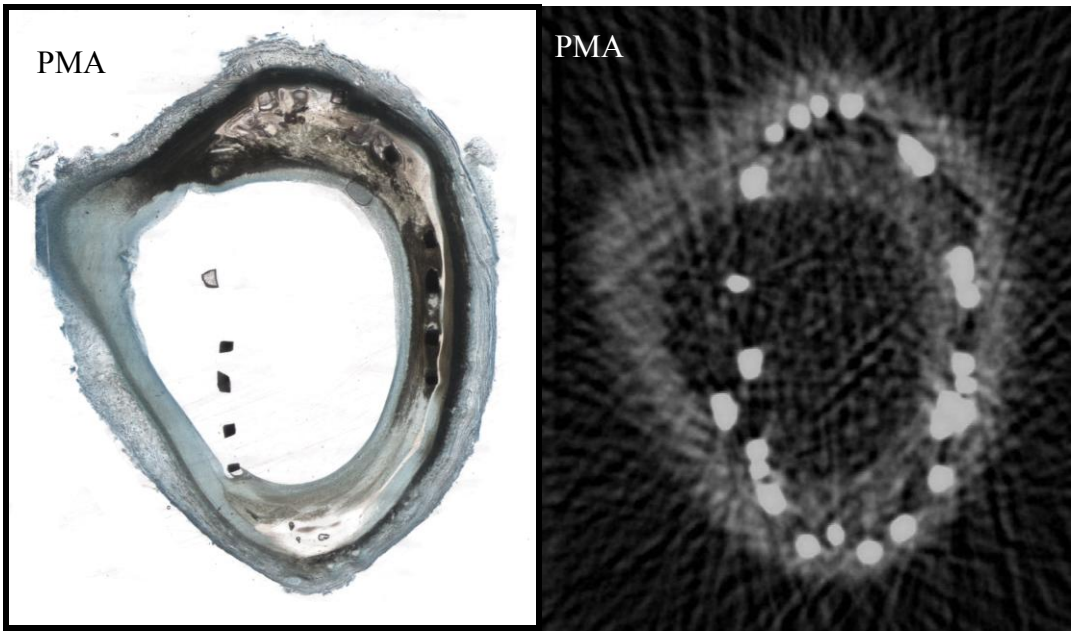

Figure 5. PMA Staining for 48 Hrs
Comparison of histology (left) and microCT slice view (right) of a vessel having been stained with PMA. The microCT slice view highlights the inability of PMA to sufficiently increase the soft tissue contrast to mask the metal streaking artifacts.

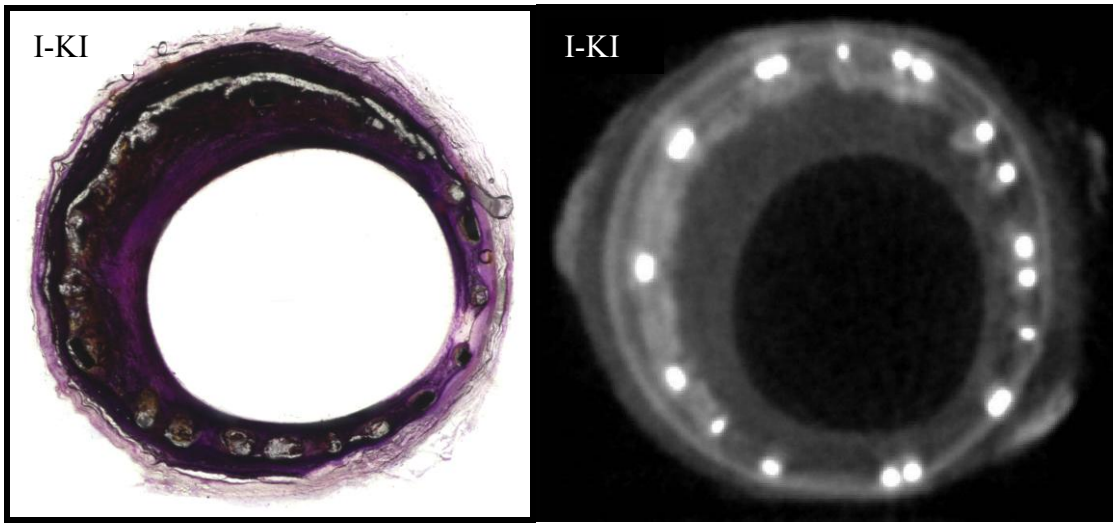

Figure 6. I-KI Staining for 48 Hrs
Comparison of histology (left) and microCT slice view (right) of a vessel having been stained with I-KI. The I-KI stain was not removed before processing for histology and thus there is some artifact from the I-KI interfering with the embedding process.

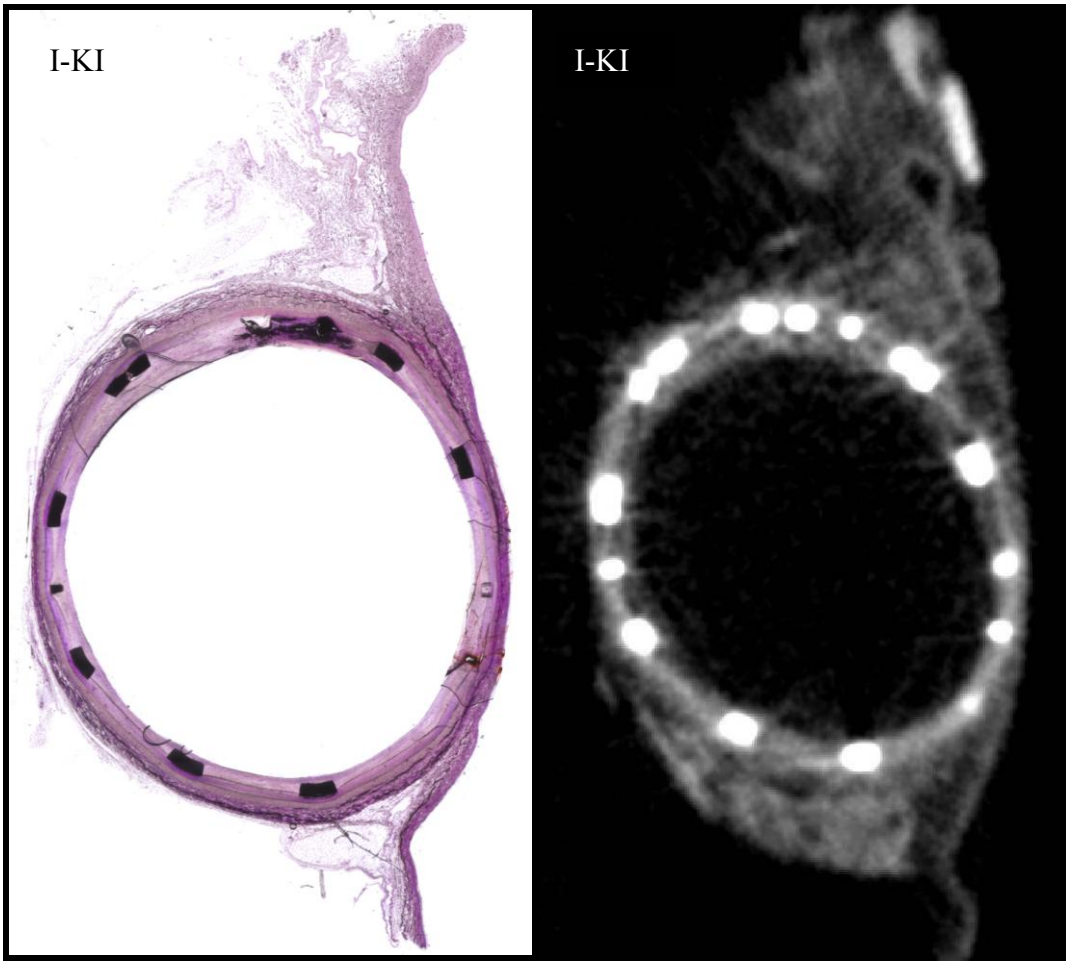

Figure 7. I-KI Staining for 3 Hrs
Comparison of histology (left) and microCT slice view (right) of a vessel having been stained with I-KI for 3 hours. The vessel was placed in formalin after scanning and allowed to sit for 24 hours before being processed for histology. The speed and utility of this technique is most clearly demonstrated here.

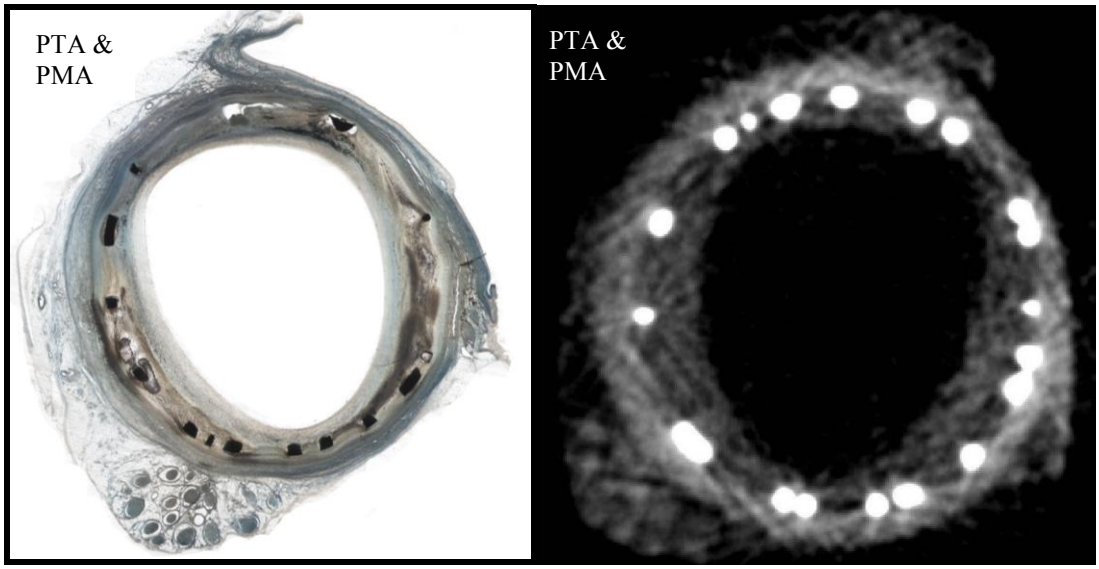

Figure 8. PTA & PMA Staining for 48 Hrs
Comparison of histology (left) and microCT slice view (right) of a vessel having been stained with PTA and PMA. Of note, the stain also was able to detect nerve tissue in the bottom left corner.

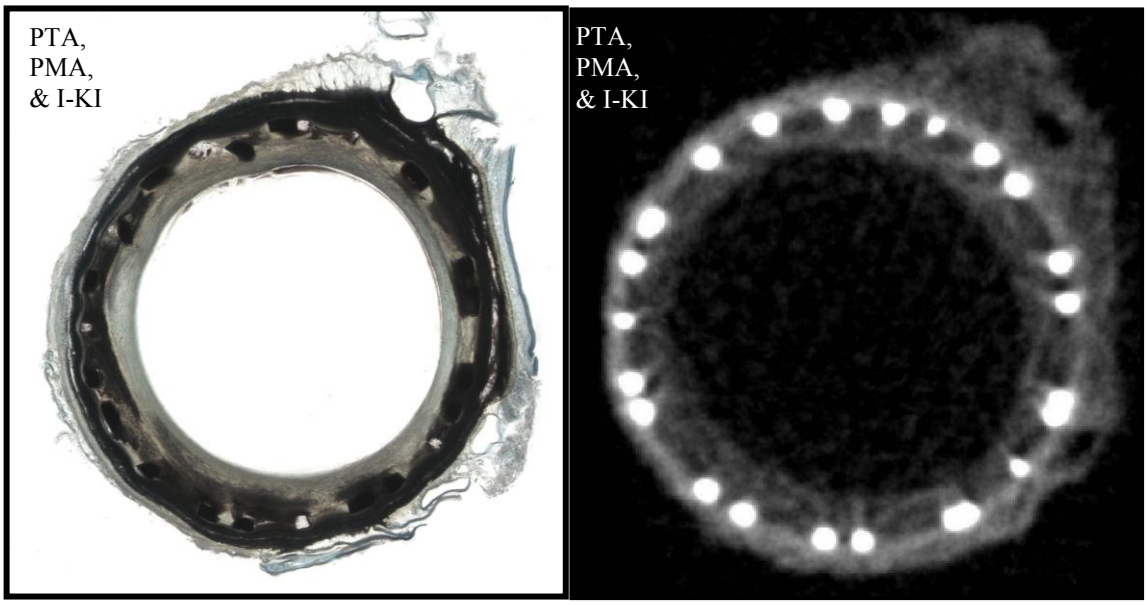

Figure 9. PTA, PMA, & I-KI Staining for 48 Hrs
Comparison of histology (left) and microCT slice view (right) of a vessel having been stained with PTA, PMA, and I-KI sequentially. The I-KI stain was not removed before processing for histology and thus, there is some artifact from the I-KI interfering with the embedding process.

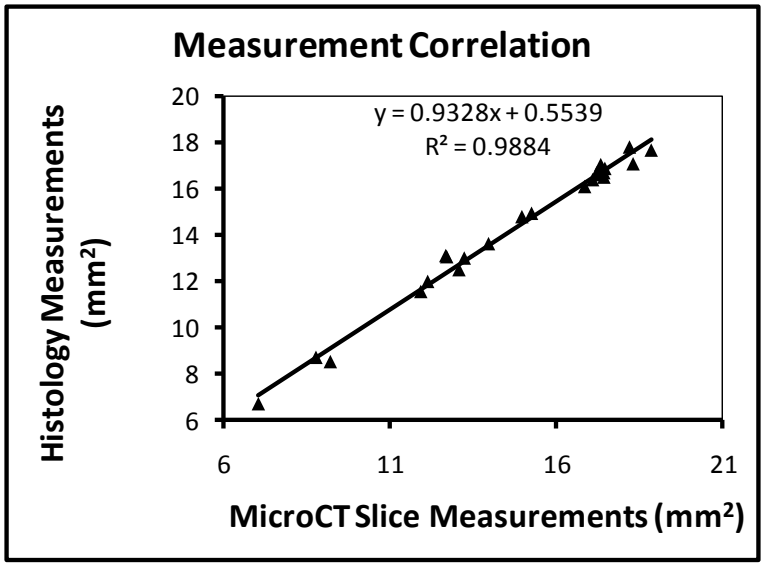

Figure 10. Correlation between Slice Measurements
Histology and microCT slice data measurements show the ability of microCT to provide accurate morphological data.

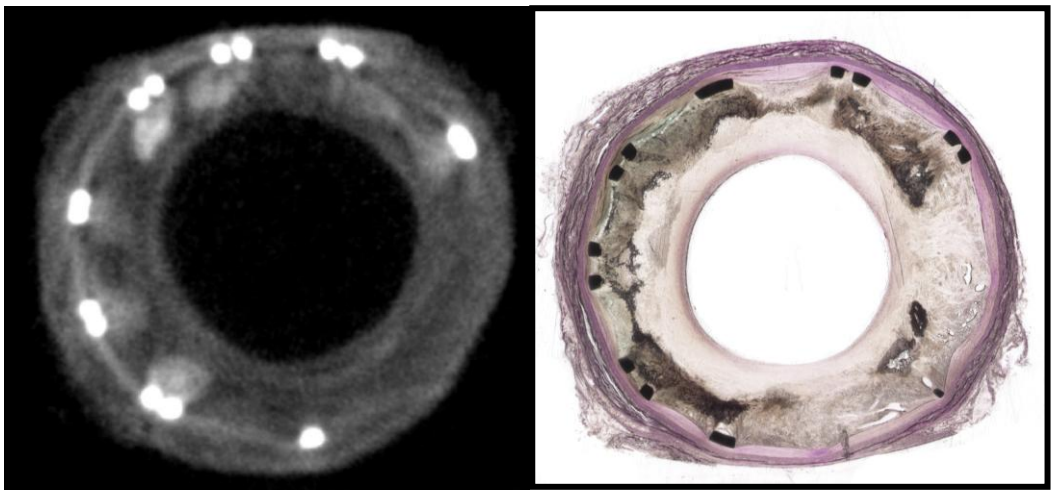

Figure 11. PAM Detected in the Vessel Walls
Both the PTA (left) and I-KI (right) based stains were able to detect PAM within the vessel wall. The areas of high stain uptake between and around the stent struts are visible in the microCT slice (white blotches) and in the histology slide (gray blotches) in areas of high neointimal growth.

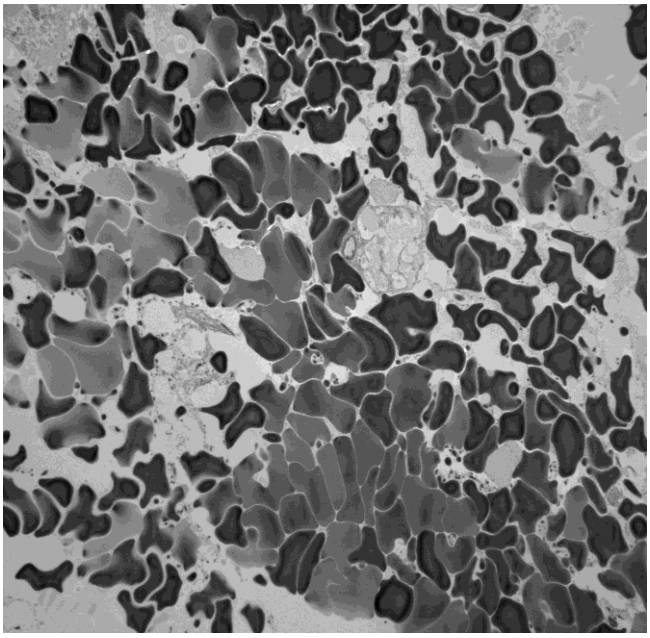

Figure 12. TEM Identification of PAM
TEM image captured of the PAM present in the vessel wall. There are red blood cells present along with macrophages.

VITA

Stephen Daniel Darrouzet received his Bachelor of Science degree in biomedical engineering from Texas A&M University in 2009. He entered a graduate program in biomedical engineering in the fall of 2009 also at Texas A&M University and received his Master of Science degree in May of 2011. His research interests include medical device development and translational research through innovative imaging techniques. He plans to apply the skills he has learned through his education to the furthering the possible applications of microCT technology among other imaging techniques.

Mr. Darrouzet may be reached at the Department of Biomedical Engineering c/o Dr. Fred Clubb, Jr. Texas A&M University, College Station, TX 77843-3120. His email address is SDarrouzet@gmail.com.